Available online at www.sciencedirect.com
SCIENCE DIRECT
International Journal of Heat and Mass Transfer 49 (2006) 1472–1479
International Journal of HEAT and MASS TRANSFER
www.elsevier.com/locate/ijhmt

Modeling for predicting frosting behavior of a fin–tube heat exchanger

Dong-Keun Yang [a], Kwan-Soo Lee [b,*], Simon Song [b]

[a] Digital Appliance Research Laboratory, LG Electronics Inc., 222-22 Guro3-dong, Seoul 152-848, Republic of Korea
[b] School of Mechanical Engineering, Hanyang University, 17 Haengdang-dong, Sungdong-gu, Seoul 133-791, Republic of Korea

Received 14 August 2005; received in revised form 6 September 2005
Available online 22 November 2005

Abstract

A mathematical model is proposed to evaluate the frosting behavior of a fin–tube heat exchanger under frosting conditions. Empirical correlations of the heat transfer coefficients for the plate and tube surfaces and a diffusion equation for the frost layer are used to establish the model. The correlations for the heat transfer coefficients, derived from various experimental data, were obtained as functions of the Reynolds number and Prandtl number. The proposed model is validated by comparing the numerical results with experimental data for the frost thickness, frost accumulation, and heat transfer rate. The numerical results agree well with the experimental data. It is also found that this model can be applied to evaluate the thermal performance of a common fin–tube heat exchanger under frosting conditions.

Keywords: Heat and mass transfer; Frost; Fin–tube heat exchanger

1. Introduction

Frost formation on the cold surface of a heat exchanger operated under frosting conditions causes a decrease in the air-flow rate and an increase in the frost surface temperature resulting in reduced thermal performance. Since frost formation strongly affects the performance of a heat exchanger for low-temperature applications, development of a frosting model to predict the frost growth is required.

Previous studies on frost formation can be categorized into two groups: one using a basic geometry, such as a flat plate or cylindrical surface, and the other using a real heat-exchanger geometry. For the first group using locally simplified geometries, many experimental and numerical studies have been performed under various frosting conditions. Some of studies in this group investigated the heat and mass transfer and frost growth on a cold plate and cylinder surface numerically and validated the numerical models with experimental data [1–10]. Other studies proposed empirical correlations for the frost properties after performing experiments for various frosting parameters [11–16]. Therefore, frost formation on flat plate and cylindrical surface is relatively well known and can be predicted reliably with existing models and correlations.

Experimental studies have also been conducted for the second group using heat exchangers for industrial and domestic refrigerators. The studies in this group include the effects of surface treatments on frosting behavior [17] and the thermal performance of a heat exchanger under various operating conditions [18,19]. However, analytical studies for the thermal performance of a heat exchanger [20–23] dealt with the frost formation phenomena too simplistically by either proposing models without robust validations or using correlations for heat transfer coefficients that were derived for a specific heat exchanger experimentally. Therefore, it is undesirable to apply the results of these studies to applications that a different shape of heat exchanger is considered.

There is a strong demand for development of numerical models to evaluate the thermal performance of heat

* Corresponding author. Tel.: +82 2 2220 0426; fax: +82 2 2295 9021.
E-mail address: ksleehy@hanyang.ac.kr (K.-S. Lee).

0017-9310/$ - see front matter © 2005 Elsevier Ltd. All rights reserved.
doi:10.1016/j.ijheatmasstransfer.2005.09.022

Nomenclature

A	area [m^2]
BR	blockage ratio [%]
c_p	specific heat at constant pressure [J/kg K]
D	mass diffusivity [m^2/s]
D_h	hydraulic diameter [mm]
d_i	inner diameter of the tube [mm]
G	mass flow rate per unit area [kg/m^2 s]
h_{fg}	latent heat of evaporation [J/kg]
$\overline{h}_h$	heat transfer coefficient [W/m^2 K]
$\overline{h}_m$	mass transfer coefficient [kg/m^2 s]
h_{sv}	latent heat of sublimation [J/kg]
k	thermal conductivity [W/m K]
$k_{f,eff}$	effective thermal conductivity of frost [W/m K]
L	length of the cooling plate [mm]
Le	Lewis number, α/D
$\dot{m}$	mass flow rate [kg/m^2 s]
m''	mass flux [kg/s]
$\overline{Nu}$	Nusselt number
P_f	fin spacings [mm]
Pr	Prandtl number
Q	heat transfer rate [W]
R	radius of the tube [mm]
Re	Reynolds number
T	temperature [K]
t	time [s]
W	length of an infinitesimal tube [mm]
w_a	absolute humidity [kg/kg_a]
x	quality of refrigerant
y	frost layer thickness [mm]

Greek symbols

α_f	absorption factor [s^{-1}]
Δ	increment
η	fin efficiency
μ	viscosity [kg/m s]
ρ	density [kg/m^3]

Superscripts

t	time
Δt	time increment

Subscripts

a	air
ave	average
cond	conduction
f	frost
fin	fin
fs	frost surface
in	inlet
l	liquid
lat	latent
n	number of tube
out	outlet
r	refrigerant
sen	sensible
tot	total
tube	tube
v	vapor
w	water–vapor
y	frost thickness
ρ	frost density

exchangers. Although several studies have examined frosting performance, they have been performed experimentally, and most of the results are applicable only to individual heat exchangers. An effective frosting model for predicting the thermal performance of a fin–tube heat exchanger has not been developed. Consequently, the prediction of frost growth in a heat exchanger under various operating conditions requires numerous prototypes of the heat exchanger and experiments wasting time, effort and cost. This results in an ineffective design process for heat exchangers.

This paper proposes a mathematical model to predict the frosting behavior on a fin–tube heat exchanger under various frosting conditions. Frost formations are experimentally studied on cold plate and cylinder surfaces to derive correlations of the heat transfer coefficients. Experiments for a fin–tube heat exchanger are also performed to validate the model.

2. Experiments

Frosting experiments were conducted to derive correlations of the heat transfer coefficients on cold plate and cylinder surfaces with frost layers formed. In order to validate the proposed model, the frosting rate, frost mass and heat transfer rate were measured for simple (2-column and 2-row) and typical (2-column and 8-row) fin–tube heat exchangers. The geometric parameters of the heat exchangers are shown in Tables 1 and 2.

The experimental apparatus consisted of a climate chamber controlling the temperature and humidity of the air at a constant value, a refrigeration section regulating the temperature and flow rate of the refrigerant, a test section where frost formation occurs, and a circulation section controlling the flow rate of the humid air and connecting each section of the apparatus. Each section of the apparatus was controlled individually [16].

Table 1
Geometric parameters of a 2-column, 2-row fin–tube heat exchanger

Parameters	Values
Fin width (mm)	60
Fin length (mm)	27
Fin thickness (mm)	0.2
Fin spacing (mm)	
Row 1,2	20
Number of columns	2
Number of rows	2
Tube length (mm)	370
Outer tube diameter (mm)	8.0
Transverse tube spacing (mm)	27
Longitudinal tube spacing (mm)	30

Table 2
Geometric parameters of a 2-column, 8-row fin–tube heat exchanger

Parameters	Values
Fin width (mm)	60
Fin length (mm)	27
Fin thickness (mm)	0.15
Fin spacing (mm)	
Row 1,2	20
Row 3,4	10
Row 5.6	7.5
Row 7,8	5
Number of columns	2
Number of rows	8
Tube length (mm)	440
Outer tube diameter (mm)	8.5
Transverse tube spacing (mm)	25
Longitudinal tube spacing (mm)	30

The climate chamber had Pt 100 Ω RTD sensors in a dry/wet bulb thermometer to measure the temperature and humidity of the air, and used the PID controller, heater, cooler, and humidifier to regulate the air temperature and humidity. The refrigeration section consisted of a refrigerator to cool the refrigerant and a pump to circulate the refrigerant. The refrigerant was a mixture of ethyleneglycol and distilled water in a mass ratio of 6:4. The air temperature and humidity were measured at the inlet and outlet of the test section by ten type-T thermocouples, a thermopile, and humidity sensors. A blower with an inverter was used to regulate the air-flow rate, and the rate was measured using a nozzle-type flowrate meter. To make the air-flow homogenous, honeycombs and air-mixing fans were installed at the inlet and outlet of the test section. In addition, insulation was attached to the surface of the experimental apparatus to minimize the heat loss.

Before performing the experiments, the climate chamber was operated to control the air-flow conditions. When air conditions reached a steady state, the frosting experiments were started by running the refrigerator and pump. The experimental data for the air and refrigerant were recorded every four second by a data recording system and a computer.

Using the air-flow rate and the absolute humidity difference between the inlet and outlet of the test section, the frosting rate was calculated as

$$\dot{m}_f = \dot{m}_a(w_{a,in} - w_{a,out}) \tag{1}$$

The heat transfer rate of the air and refrigerant was estimated from

$$Q_{tot} = \dot{m}_a c_{p,a}(T_{a,in} - T_{a,out}) + \dot{m}_f h_{sv} \quad \text{for the air} \tag{2}$$

$$Q_{tot} = \dot{m}_r c_{p,r}(T_{r,out} - T_{r,in}) \quad \text{for the refrigerant} \tag{3}$$

During the experiments, the energy balance between the air and refrigerant was maintained within 5%, as stated in ASHRAE Standard 33–78.

The heat transfer coefficients for the frost surface of the cold plate and cylinder were calculated using:

$$\bar{h}_h = \frac{\dot{m}_a c_{p,a}(T_{a,in} - T_{a,out})}{A_{tot}(T_{a,ave} - T_{fs})} \tag{4}$$

Uncertainties of the experimental data were computed by considering the bias error and accuracy of the used equipments [24]. The uncertainties of the average frost thickness, frost mass, heat transfer rate, and heat transfer coefficient were estimated as 5.28%, 4.50%, 3.69%, and 5.07%, respectively.

3. Mathematical modeling and calculation procedure

This paper presents a mathematical model for predicting the frosting behavior of a fin–tube heat exchanger and evaluates the thermal performance of the heat exchanger under frosting conditions. To perform the numerical analysis, the heat exchanger is divided into infinitesimal control volumes in the direction of the air-flow, refrigerant flow, and the normal to the flow plane. The assumptions in each infinitesimal control volume are as follows:

(1) The frost layers that formed on the fin and tube surfaces of each infinitesimal control volume are homogeneous, respectively.
(2) The frosting process takes place at a quasi-steady state.
(3) The local frosting behavior at junctions of the fin and tube is not considered.
(4) The heat transfer mechanism inside the frost layer is conduction, and the effective thermal conductivity of the frost layer is a function of the frost density.

3.1. Mathematical modeling

In order to predict the frost growth in the heat exchanger, the modeling is performed on two parts separately: fin and tube parts. Fig. 1 shows a schematic diagram of the heat exchanger.

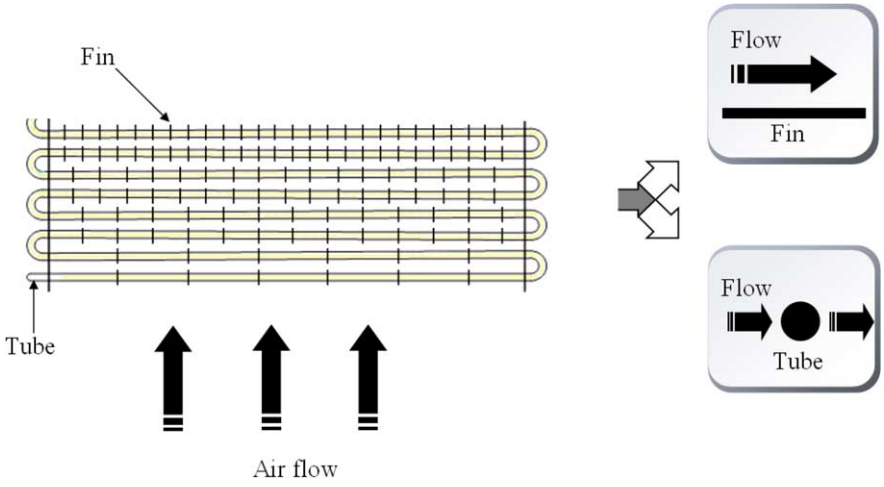

Fig. 1. Schematic diagram of a general fin–tube heat exchanger.

Sensible and latent heat transfers between the surfaces of the heat exchanger and the moist air inside the infinitesimal control volumes are calculated as

$$\begin{aligned} Q_{\text{sen}} &= Q_{\text{sen,fin}} + Q_{\text{sen,tube}} \\ &= \eta_{\text{fin}}\overline{h}_{\text{h,fin}}A_{\text{fin,f}}(T_{\text{a}} - T_{\text{fin,fs}}) + \overline{h}_{\text{h,tube}}A_{\text{tube,f}}(T_{\text{a}} - T_{\text{tube,fs}}) \end{aligned} \quad (5)$$

$$\begin{aligned} Q_{\text{lat}} &= Q_{\text{lat,fin}} + Q_{\text{lat,tube}} \\ &= \eta_{\text{fin}}\overline{h}_{\text{m,fin}}A_{\text{fin,f}}(w_{\text{a}} - w_{\text{fin,fs}})h_{\text{sv}} + \overline{h}_{\text{m,tube}}A_{\text{tube,f}}(w_{\text{a}} - w_{\text{tube,fs}})h_{\text{sv}} \end{aligned} \quad (6)$$

where η_{fin} is the fin efficiency defined by Schmidt [25]. The mass transfer coefficients inside the infinitesimal control volumes are computed using analogy between heat and mass transfer:

$$\overline{h}_{\text{m}} = \frac{\overline{h}_{\text{h}}}{c_{\text{p,a}}Le^{2/3}} \quad (7)$$

The conduction heat transfer inside the frost layer that formed on the fin and tube is calculated using

$$Q_{\text{cond,fin}} = k_{\text{f,eff}}A_{\text{fin,f}}\left(\frac{T_{\text{fin,fs}} - T_{\text{fin}}}{y_{\text{fin,f}}}\right) \quad (8)$$

$$Q_{\text{cond,tube}} = 2\pi k_{\text{f,eff}}W\left[\frac{T_{\text{tube,fs}} - T_{\text{tube}}}{\ln[(R + y_{\text{tube,f}})/R]}\right] \quad (9)$$

where the effective thermal conductivity of the frost layer is determined as [26]

$$k_{\text{f,eff}} = 1.202 \times 10^{-3}\rho_{\text{f}}^{0.963} \quad (10)$$

The heat transfer from the air should be balanced with the conduction heat transfer in the frost layer that formed on the fin and tube as follows:

$$Q_{\text{cond,fin}} = Q_{\text{sen,fin}} + Q_{\text{lat,fin}} \quad (11)$$

$$Q_{\text{cond,tube}} = Q_{\text{sen,tube}} + Q_{\text{lat,tube}} \quad (12)$$

The surface temperatures of the frost layer that formed on the fin and tube are determined considering the energy balance at the frost surface:

$$T_{\text{fin,fs}} = \frac{\eta_{\text{fin}}\overline{h}_{\text{h,fin}}A_{\text{fin,f}}T_{\text{a}} + \eta_{\text{fin}}\overline{h}_{\text{m,fin}}A_{\text{fin,f}}(w_{\text{a}} - w_{\text{fin,fs}})h_{\text{sv}} + k_{\text{f,eff}}A_{\text{fin,f}}\frac{T_{\text{fin}}}{y_{\text{fin,f}}}}{\frac{k_{\text{f,eff}}A_{\text{fin,f}}}{y_{\text{fin,f}}} + \eta_{\text{fin}}\overline{h}_{\text{h,fin}}A_{\text{fin,f}}} \quad (13)$$

$$T_{\text{tube,fs}} = \frac{\overline{h}_{\text{h,tube}}A_{\text{tube,f}}T_{\text{a}} + \overline{h}_{\text{m,tube}}A_{\text{tube,f}}(w_{\text{a}} - w_{\text{tube,fs}})h_{\text{sv}} + \frac{2\pi k_{\text{f,eff}}WT_{\text{tube}}}{\ln[(R+y_{\text{tube,f}})/R]}}{\frac{2\pi k_{\text{f,eff}}W}{\ln[(R+y_{\text{tube,f}})/R]} + \overline{h}_{\text{h,tube}}A_{\text{tube,f}}} \quad (14)$$

This study uses a water–vapor diffusion equation in the frost layer to predict the frost growth on the fin–tube heat exchanger. Previous numerical studies of the frost formation on a simple geometry, such as a flat plate or cylinder, used either a water–vapor diffusion equation [1,2,4] or a correlation for the frost density [5,6]. In our case, the temperature and humidity of the moist air varies along the air-flow direction due to the frost formation although the temperature and humidity of the air at the inlet of the heat exchanger is maintained as a constant value. Fig. 2 shows a schematic diagram of the temperature and humidity

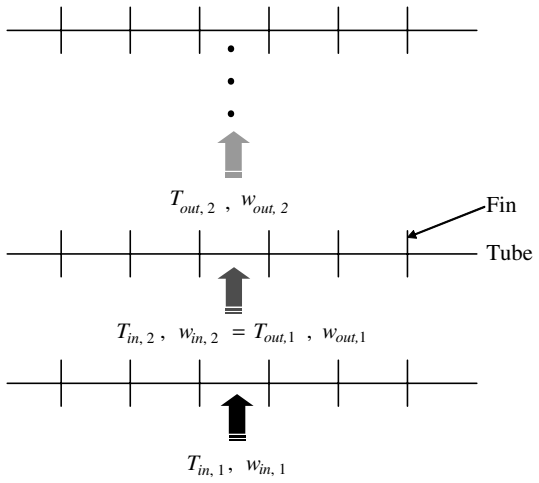

Fig. 2. Temperature and humidity variations in the air-flow direction.

variation of the air. This variation requires a frost density correlation for a broad range of experimental conditions. Unfortunately, the frost density correlations proposed in the previous studies do not consider the temperature and humidity variation of the moist air in the flow direction. Therefore, the following diffusion equation [2] is used in the present study assuming that the amount of water–vapor absorbed into a control volume inside the frost layer is proportional to the water–vapor density

$$D\frac{d^2\rho_w}{dy^2} = \alpha_f \rho_w \tag{15}$$

The water–vapor is transferred from the moist air to the frost layer through the surface. The total mass flux that increases the frost density and layer thickness can be expressed as

$$\begin{aligned} m''_f &= m''_{fin,f} + m''_{tube,f} = m''_{fin,y} + m''_{fin,\rho} + m''_{tube,y} + m''_{tube,\rho} \\ &= \eta_{fin}\overline{h}_{m,fin}(w_a - w_{fin,fs}) + \overline{h}_{m,tube}(w_a - w_{tube,fs}) \end{aligned} \tag{16}$$

The mass fluxes increasing the frost density are given as

$$\begin{aligned} m''_{fin,\rho} &= \int_{y=0}^{y=y_{fin,f}} \alpha_f \rho_w \, dy \\ m''_{tube,\rho} &= \int_{y=0}^{y=y_{tube,f}} \alpha_f \rho_w \, dy \end{aligned} \tag{17}$$

The frost density and layer thickness on the fin and tube at each time step are determined:

$$\begin{aligned} \rho^{t+\Delta t}_{fin,f} &= \rho^t_{fin,f} + \frac{m''_{fin,\rho}}{y_{fin,f}}\Delta t, \quad y^{t+\Delta t}_{fin,f} = y^t_{fin,f} + \frac{m''_{fin,y}}{\rho_{fin,f}}\Delta t \\ \rho^{t+\Delta t}_{tube,f} &= \rho^t_{tube,f} + \frac{m''_{tube,\rho}}{y_{tube,f}}\Delta t, \quad y^{t+\Delta t}_{tube,f} = y^t_{tube,f} + \frac{m''_{tube,y}}{\rho_{tube,f}}\Delta t \end{aligned} \tag{18}$$

The heat and mass balances at the inlet and outlet of an infinitesimal control volume are as follows:

$$Q_{sen} = \dot{m}_a c_{p,a}(T_{a,in} - T_{a,out}) \tag{19}$$

$$Q_{lat} = \dot{m}_a(w_{a,in} - w_{a,out})h_{sv} \tag{20}$$

The temperature and humidity at the outlet are obtained using Eqs. (19) and (20):

$$\begin{aligned} &T_{in,1} = T_{in}, T_{in,2} = T_{out,1}, T_{in,3} = T_{out,2}, \ldots, T_{in,n} = T_{out,n-1} \\ &w_{in,1} = w_{in}, w_{in,2} = w_{out,1}, w_{in,3} = w_{out,2}, \ldots, w_{in,n} = w_{out,n-1} \end{aligned} \tag{21}$$

The outlet conditions are used as the inlet conditions for the subsequent control volume in the air-flow direction.

The state and phase of the refrigerant in the tube varies due to the frost formation on the fin and tube. This variation causes the surface temperature of the fin and tube to changes along the tube. Neglecting the thermal resistance of tube walls, the heat transfer due to the air and refrigerant in an infinitesimal control volume should be balanced. This balance can be expressed as follows:

$$\begin{aligned} Q_{tot} &= h_r A_{tube}(T_{tube} - T_r) \\ &= \begin{cases} \dot{m}_r c_{p,r}(T_{r,out} - T_{r,in}), & \text{for single-phase region} \\ \dot{m}_r(x_{r,out} - x_{r,in})h_{fg}, & \text{for two-phase region} \end{cases} \end{aligned} \tag{22}$$

The correlations used to estimate the heat transfer coefficients are listed below:

(1) Single-phase region [27]

$$\frac{h_r d_i}{k} = 0.023 Re^{0.8} Pr^{0.4} \tag{23}$$

(2) Two-phase region($0 \leqslant x \leqslant 0.85$) [28]

$$\frac{h_r d_i}{k_l} = \begin{cases} 0.0265 Re_{eq}^{0.8} Pr_l^{1/3}, & Re_{eq} > 5\times 10^4 \\ 5.03 Re_{eq}^{1/3} Pr_l^{1/3}, & Re_{eq} < 5\times 10^4 \end{cases} \tag{24}$$

where

$$\begin{aligned} Re_{eq} &= G_{eq} d_i/\mu_l \\ G_{eq} &= G_l + G_v\left(\frac{\rho_l}{\rho_v}\right)^{1/2} \end{aligned} \tag{25}$$

(3) Two-phase region($0.85 \leqslant x \leqslant 1.0$) [27,28]

$$h_r = h_{r,x=1.0} + \frac{h_{r,x=0.85} - h_{r,x=1.0}}{0.85 - 1.0}(x - 1.0) \tag{26}$$

3.2. Calculation procedure

To predict the frosting behavior of a fin–tube heat exchanger, numerical analyses are performed according to the calculation procedure listed below:

(1) The heat exchanger is divided into infinitesimal control volumes in the direction of air-flow, refrigerant flow, and the normal to the flow plane.
(2) The tube diameter, calculation time, time increment, inlet air conditions, and temperature of the fin and tube are given, and the initial surface temperature and density of the frost layer on the fin and tube are assigned.
(3) The frost mass, frost thickness, frost density, heat and mass transfer coefficients on the fin and tube, and effective thermal conductivity of the frost layer are calculated using the properties at a film temperature.
(4) The frost surface temperature of every infinitesimal control volume is calculated.
(5) If a convergence condition for the frost surface temperature in each infinitesimal control volume is satisfied, the calculation proceeds to the next time step. If not, the calculation is iterated until the convergence condition is satisfied.

4. Results and discussion

The present study proposes a mathematical model using correlations for the heat transfer coefficients of the air-flow and a diffusion equation for the water–vapor in order to predict the frosting behavior on a fin–tube heat exchanger. To establish the mathematical model, the following correlations are used:

$$\overline{Nu}_{\mathrm{fin}} = \frac{\overline{h}_{\mathrm{h,fin}} L}{k_{\mathrm{a}}} = 0.204 Re_{L}^{0.657} Pr^{1.334} \tag{27}$$

$$\overline{Nu}_{\mathrm{tube}} = \frac{\overline{h}_{\mathrm{h,tube}} D_{\mathrm{h}}}{k_{\mathrm{a}}} = 0.146 Re_{D_{\mathrm{h}}}^{0.917} Pr^{2.844} \tag{28}$$

where the heat transfer coefficients were obtained from experiments.

To validate the proposed frosting model, Fig. 3 compares the numerical results with the experimental data for the frost thickness on a 2-column, 2-row fin–tube heat exchanger. The numerical results are in good agreement with the experimental data although there is a slight discrepancy in the initial time.

In general, a design of a heat exchanger under frosting conditions requires an accurate prediction of the heat transfer rate. Moreover, the frost mass should be estimated accurately to determine the amount of heat required to remove the frost. In order to evaluate the applicability of the proposed frosting model, a numerical analysis was performed for a 2-column, 8-row fin–tube heat exchanger. Fig. 4 shows a comparison of the numerical results to corresponding experimental data for the frost mass and frosting rate. The numerical results agree well with the

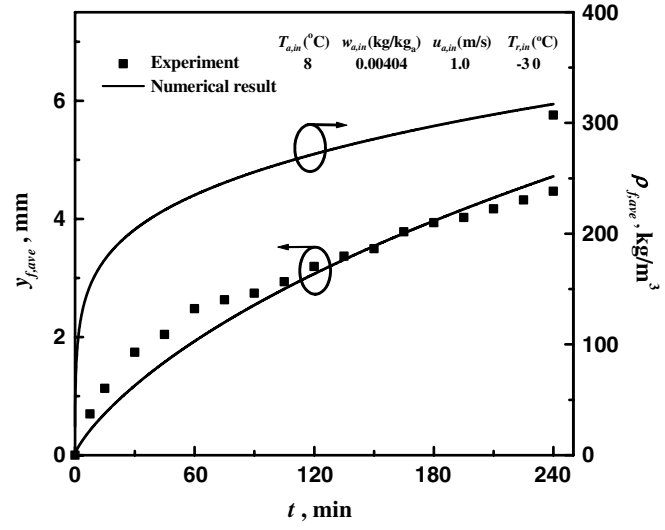

Fig. 3. Comparison of numerical results and experimental data for the average frost thickness in a 2-column, 2-row fin–tube heat exchanger.

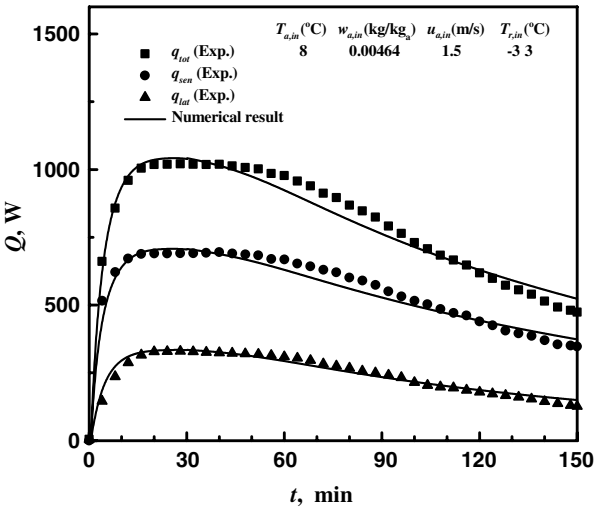

Fig. 5. Comparison of numerical results and experimental data for the heat transfer rate in a 2-column, 8-row fin–tube heat exchanger.

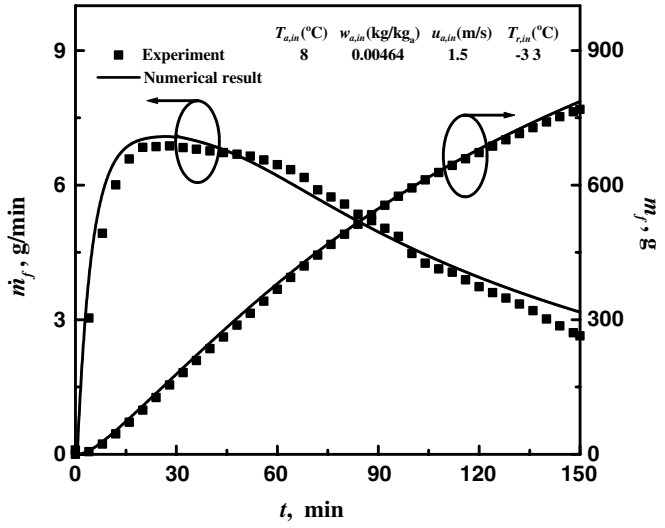

Fig. 4. Comparison of numerical results and experimental data for the frost mass and frosting rate in a 2-column, 8-row fin–tube heat exchanger.

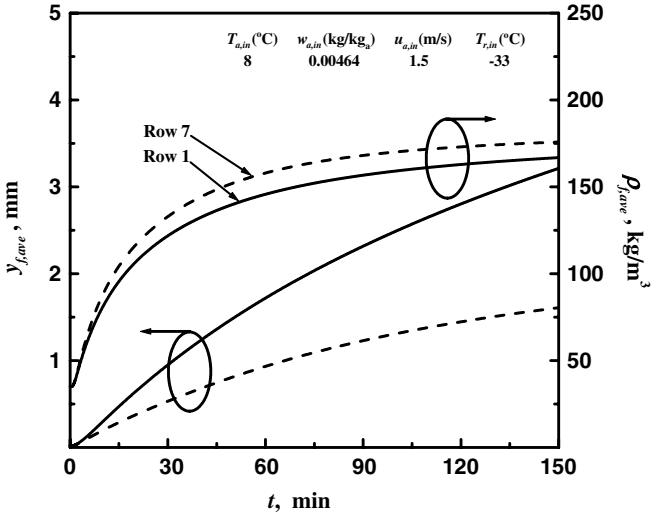

Fig. 6. Average frost thickness and density in the first and the seventh rows of a 2-column, 8-row fin–tube heat exchanger.

Table 3
Ratios of heat transfer area and average heat transfer rate in each row to the total values of a 2-column, 8-row fin–tube heat exchanger

	Row 1	Row 2	Row 3	Row 4	Row 5	Row 6	Row 7	Row 8
A_n/A_{tot}	0.063	0.063	0.107	0.107	0.135	0.135	0.195	0.195
$Q_{ave,n}/Q_{ave,tot}$	0.109	0.104	0.134	0.124	0.134	0.123	0.143	0.129

experimental data. The difference between the predicted and actual frost mass at $t = 180$ min is only 2.2%.

Fig. 5 compares the numerical results with experimental data for the heat transfer rate. Despite a decreased air-flow rate due to the frost formation, the heat transfer rate does not vary significantly for the first 60 min because of the increased heat transfer area and enhanced air-flow disturbance. The predicted latent heat transfer rate is in good agreement, as implied in Fig. 4, but the sensible heat transfer rate is slightly under-predicted around the 80-min time point. Nevertheless, the overall numerical results for the heat transfer rate agree well with the experimental data.

Fig. 6 presents the average frost thickness and density in the first and the seventh rows of a fin–tube heat exchanger. The frost growth at the first row is promoted by the high-temperature moist air. On the other hand, the frost layer at the seventh row along air-flow direction is very thin and dense due to the low temperature and humidity of the air.

Fig. 7 shows average blockage ratios at each row of the fin–tube heat exchanger at $t = 150$ min. The blockage ratio represents an extent of air-flow blocking between fins of a heat exchanger and affects the thermal performance of the heat exchanger because of its close relation to the air-flow rate. According to the reference [17], the ratio is defined as

$$\mathrm{BR}_{\mathrm{ave}} = 2 \times \left(\frac{y_{\mathrm{f,ave}}}{P_{\mathrm{f}}} \right) \times 100 \tag{29}$$

where $y_{\mathrm{f,ave}}$ and P_{f} represent the average frost thickness and fin spacing, respectively.

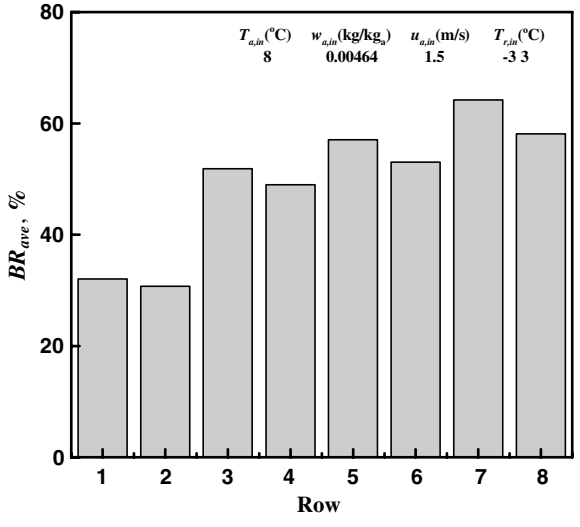

Fig. 7. Average blockage ratios in each row of a 2-column, 8-row fin–tube heat exchanger at $t = 150$ min.

As shown in Fig. 7, the blockage ratio is highest in the seventh row. The air-flow passage in the seventh row with a small fin spacing is quickly blocked by the frost layer formed on the surface of the fins, decreasing the air-flow rate and degrading the thermal performance of the heat exchanger.

Table 3 presents ratios of heat transfer area and average heat transfer rate in each row to the total values of the heat exchanger. The heat transfer in the seventh and the eighth rows is not efficient despite large heat transfer area. Therefore, the thermal performance of the heat exchanger can be improved by the proper adjustment of fin spacing. For example, decreasing the fin spacing in the rows 1–4 and increasing the spacing in the rows 5–8 would improve the thermal performance of the heat exchanger by reducing the air-flow blocking.

5. Conclusions

This paper proposed a mathematical model to predict the thermal performance of a fin–tube heat exchanger under frosting conditions. The correlations for the heat transfer coefficients for frost layer formed on cold plate and cylinder surfaces were derived from experimental data. Experiments were performed to acquire benchmark data to validate the mathematical model. The model was developed using correlations for the heat transfer coefficients on the fin and tube and a water–vapor diffusion equation for the frost layer. The results of the proposed model accurately predicted the frost growth and heat transfer rate and agreed well with the experimental data. This implies that the model can be used to predict the thermal performance of a fin–tube heat exchanger with multiple columns and rows.

Acknowledgement

This research was supported by The Center of Innovative Design Optimization Technology (iDOT), Korea Science and Engineering Foundation.

References

[1] B.W. Jones, J.D. Parker, Frost formation with varying environmental parameters, J. Heat Transfer 97 (1975) 255–259.
[2] K.S. Lee, W.S. Kim, T.H. Lee, A one-dimensional model for frost formation on a cold flat surface, Int. J. Heat Mass Transfer 40 (18) (1997) 4359–4365.
[3] R. Yun, Y. Kim, M.K. Min, Modeling of frost growth and frost properties with airflow over a flat plate, Int. J. Refrig. 25 (3) (2002) 362–371.

[4] K.S. Lee, S. Jhee, D.K. Yang, Prediction of the frost formation on a cold flat surface, Int. J. Heat Mass Transfer 46 (20) (2003) 3789–3796.
[5] P.J. Mago, S.A. Sherif, Heat and mass transfer on a cylinder surface in cross flow under supersaturated frosting conditions, Int. J. Refrig. 26 (8) (2003) 889–899.
[6] S.P. Raju, S.A. Sherif, Frost formation and heat transfer on circular cylinders in cross-flow, Int. J. Refrig. 16 (6) (1993) 390–401.
[7] K.A.R. Ismail, C.S. Salinas, Modeling of frost formation over parallel cold plates, Int. J. Refrig. 22 (5) (1999) 425–441.
[8] R. LeGall, J.M. Grillot, C. Jallut, Modelling of frost growth and densification, Int. J. Heat Mass Transfer 40 (13) (1997) 3177–3187.
[9] H. Chen, R.W. Besant, Y.X. Tao, Frost characteristics and heat transfer on a flat plate under freezer operating conditions. Part II: Numerical modeling and comparison with data, ASHRAE Trans. 105 (1) (1999) 252–259.
[10] B. Na, R.L. Webb, New model for frost growth rate, Int. J. Heat Mass Transfer 47 (5) (2004) 925–936.
[11] H.W. Schneider, Equation of the growth rate of frost forming on cooled surfaces, Int. J. Heat Mass Transfer 21 (1978) 1019–1024.
[12] R. Östin, S. Anderson, Frost growth parameters in a forced air stream, Int. J. Heat Mass Transfer 14 (4/5) (1991) 1009–1017.
[13] J.D. Yonko, C.F. Sepsy, An investigation of the thermal conductivity of frost while forming on a flat horizontal plate, ASHRAE Trans. 73 (2) (1967) 1.1–1.11.
[14] Y. Mao, R.W. Besant, H. Chen, Frost characteristics and heat transfer on a flat plate under freezer operating conditions. Part 1: Experimentation and correlations, ASHRAE Trans. 105 (2) (1999) 231–251.
[15] Y. Hayashi, A. Aoki, S. Adachi, K. Hori, Study of frost properties correlation with frost formation types, ASME J. Heat Transfer 99 (1977) 239–245.
[16] D.K. Yang, K.S. Lee, Dimensionless correlations of frost properties on a cold plate, Int. J. Refrig. 27 (1) (2004) 89–96.
[17] S. Jhee, K.S. Lee, W.S. Kim, Effect of surface treatments on the frosting/defrosting behavior of a fin-tube heat exchanger, Int. J. Refrig. 25 (8) (2002) 1047–1053.
[18] W.M. Yan, H.Y. Li, Y.J. Wu, J.Y. Lin, W.R. Chang, Performance of finned tube heat exchangers operating under frosting conditions, Int. J. Heat Mass Transfer 46 (5) (2003) 871–877.
[19] D. Deng, L. Xu, S. Xu, Experimental investigation on the performance of air cooler under frosting conditions, Appl. Therm. Eng. 23 (8) (2003) 905–912.
[20] S.N. Kondepudi, D.L. ON'eal, Performance of finned-tube heat exchangers under frosting conditions: I. Simulation model, Int. J. Refrig. 16 (3) (1993) 175–180.
[21] Y. Yao, Y. Jiang, S. Deng, Z. Ma, A study on the performance of the airside heat exchanger under frosting in an air source heat pump water heater/chiller unit, Int. J. Heat Mass Transfer 47 (17/18) (2004) 3745–3756.
[22] D. Seker, H. Karatas, N. Egrican, Frost formation on fin-and-tube heat exchangers. Part I – Modeling of frost formation on fin-and-tube heat exchangers, Int. J. Refrig. 27 (4) (2004) 367–374.
[23] Y. Xia, A.M. Jacobi, An exact solution to steady heat conduction in a two-dimensional slab on a one-dimensional fin: application to frosted heat exchangers, Int. J. Heat Mass Transfer 47 (14–16) (2004) 3317–3326.
[24] S.J. Kline, F.A. McClintock, Describing uncertainties in single-sample experiments, Mech. Eng. 75 (1953) 3–8.
[25] T.E. Schmidt, Heat transfer calculations for extended surfaces, Refrig. Eng. 57 (1949) 351–357.
[26] C.T. Sanders, The influence of frost formation and defrosting on the performance of air coolers, Ph.D. Thesis, Delft Technical University, 1974.
[27] F.P. Incropera, D.P. DeWitt, Fundamental of Heat and mass transfer, John Wiley and Sons Inc., 2002, pp. 491–492.
[28] W.W. Akers, H.A. Deans, O.K. Crosser, Condensing heat transfer within horizontal tubes, Chem. Eng. Progr. Symp. 55 (29) (1959) 171–176.